농학석사학위논문

애기장대 유래 DAO1 의 결정화 및 구조 규명

Crystallization and structure determination of DAO1 from *Arabidopsis thaliana*

2018 년 8 월

서울대학교 대학원
농생명공학부 응용생명화학전공
진 소 희

Abstract

Indole-3-acetic acid (IAA), the major form of the plant hormone auxin, regulates almost every aspect of plant growth and development. Therefore, auxin homeostasis is an essential issue in plants. Various pathways of synthesis, transport, conjugation, and catabolism are involved in auxin homeostasis, but its catabolic pathway has remained elusive until recent studies elucidated the presence of *DIOXYGENASE FOR AUXIN OXIDATION (DAO)* from *Oryza sativa* and *Arabidopsis thaliana*. DAO, a member of the 2-oxoglutarate/Fe(II)-dependent oxygenase family, constitutes a major enzyme for IAA catabolism. It catalyzes, with the cosubstrate 2-oxoglutarate, the conversion of IAA into 2-oxoindole-3-acetic acid, a functionally inactive oxidative product of IAA. Here, I report a crystal structure of the unliganded DAO1 from *A. thaliana* (AtDAO1) and its complex with 2-oxoglutarate. AtDAO1 is structurally homologous with members of the 2-oxoglutarate/Fe(II)-dependent oxygenase family but exhibits unique features in the prime substrate-binding site. Using liquid chromatography-tandem mass spectrometry analyses of the reaction products from various mutant enzymes, I provide structural insights into a putative binding site for the prime substrate IAA, thereby suggesting possible structural determinants for the substrate specificity of AtDAO1 toward IAA.

Key words: *Arabidopsis thaliana,* AtDAO1, dioxygenase for auxin oxidation, indole-3-acetic acid, 2-oxoglutarate, 2-oxoglutarate/Fe(II)-dependent oxygenase family, 2-oxoindole-3-acetic acid

Student Number: 2016-24638

Contents

List of Figures

List of Tables

List of Abbreviation

AtDAO1	*Arabidopsis thaliana* gene dioxygenase for auxin oxidation 1
IAA	indole-3-acetic acid
oxIAA	2-oxoindole-3-acetic acid
DSBH	double-stranded β-helix
2OG	2-oxoglutarate
2ODO	2-oxoglutarate/Fe(II)-dependent oxygenase
T7H	thymine-7-hydroxylase
ANS	anthocyanidin synthase
IPTG	isopropyl β-D-L-thiogalactopyranoside
Tris	tris(hydroxymethyl)aminomethane
HEPES	4-(2-hydroxyethyl)-1-piperazineethanesulfonic acid
RMSD	root mean-square deviation

Introduction

Auxin is one of the essential hormones in plants. It has been involved in almost all steps for plant growth and development (reviewed in Abel & Theologis, 2011; Estelle et al., 2011). Naturally abundant indole-3-acetic acid (IAA) is a representative of auxin molecules bearing a chemical skeleton similar with IAA. Given the crucial physiological role of auxin throughout the life stages of plant, an optimal auxin concentration should be maintained to exert its biological effects in a spatial and temporal manner, in response to changes in endo- or exo-geneous signals, environmental stress *etc*. Therefore, maintaining auxin homeostasis is one of the central metabolic events in plants.

Auxin homeostasis is regulated in an intricate and redundant manner by different fates of IAA via synthesis, transport, conjugation, and catabolism (reviewed in Ljung, 2013; Zhang & Peer, 2017). Among those metabolic routes, IAA-inactivating catabolism that involves IAA oxidation is an emerging pathway in the regulation of IAA level. In Arabidopsis seedlings, an oxidative product of IAA has long been characterized at a concentration much higher than major IAA conjugates with amino acid(s) (Kowalczyk & Sandberg, 2001), suggesting that IAA oxidation is a major metabolic pathway but a gene(s) responsible for the conversion has been remained elusive. Recently, a gene named *DIOXYGENASE FOR AUXIN OXIDATION (DAO)* was first identified in rice (Zhao et al., 2013). DAO from rice *Oryza sativa* (OsDAO) catalyzes a conversion of IAA into 2-oxindole-3-acetic acid (oxIAA) (Fig 1A), an oxidative product no longer bearing biological functions IAA exhibits. Subsequently, sequence comparisons revealed the presence of two DAO-

like genes in *Arabidopsis thaliana*, and their products (*i.e*., AtDAO1 and AtDAO2) exhibited a proposed activity for oxIAA formation by *in vivo* and *in vitro* assays (Porco et al., 2016; Zhang et al., 2016). Together with further metabolic profiling and phenotypic studies using *AtDAO1* loss and gain of function mutant lines (Mellor et al., 2016; Porco et al., 2016; Zhang et al., 2016), all these results unanimously concluded that in *A. thaliana* AtDAO1 is a major oxygenase responsible for oxIAA formation *in vivo*, and the DAO-dependent IAA oxidation constitutes a primary catabolic pathway of IAA.

DAOs, including AtDAO1 (*At1g14130*), AtDAO2 (*At1g14120*), and OsDAO (Os04g0475600), belong to a member of the 2-oxoglutarate (2OG)/Fe(II)-dependent oxygenase (2ODO) family (Fig. 1B), but are classified to be a sub-group of the family (Porco et al., 2016; Zhang et al., 2016). All members of the 2ODO family catalyze their reactions towards a prime substrate(s), with 2OG and dioxygen as co-substrates and ferrous iron as a cofactor, and operate reactions in a conserved way involving a hi-valent iron intermediate (Herr & Hausinger, 2018). The 2ODO family continues to grow in the diversity of reaction types and substrates including proteins, DNA, RNA, lipids, amino acids, natural products, and signaling molecules. Therefore, there have been intensive efforts in understanding structural diversity of the 2ODO family accommodating a wide range of substrates, even with homologous structures (Aik et al., 2012). Recent survey also added more than two hundreds 2ODOs in plants (Hagel & Facchini, 2018), but many of those putative enzymes need further investigation for their functional assignment.

In this study, I report a crystal structure of AtDAO1 and its complex with 2OG. Structural information thus obtained, along with liquid chromatography-tandem mass spectrometry (LC-MS/MS) analysis of the reaction product from

various mutant enzymes, provide structural insights into AtDAO1 and a putative binding site of the prime substrate IAA, thereby suggesting possible structural determinants for the substrate specificity of AtDAO1 towards IAA.

Figure 1. The overall reaction scheme and sequence alignment of AtDAO1.

(*A*) Under aerobic condition, AtDAO1 catalyzes in a 2ODO-dependent manner a conversion of IAA into oxIAA, with 2OG as a co-substrate and Fe(II) as a cofactor. Succinate and CO2 are liberated as products from the co-substrate 2OG. (*B*) The amino acid sequence of AtDAO1 (*At1g14130*) is compared to other DAO homologs with the validated function, including AtDAO2 (*At1g14120*), and OsDAO (*Os04g0475600*). Highly conserved residues are shown in red and boxed in blue, while strictly conserved residues are shown with a red background. Secondary structural elements defined in an unliganded AtDAO1* are shown for the corresponding sequences. Thymine-7-hydroxylase (T7H) (PDB id 5C3Q; Li et al., 2015) and anthocyanidin synthase (ANS) (PDB id 2BRT; Welford et al., 2005), a member of the 2ODO family with high structural similarity to AtDAO1 (Z-score > 28), were also included in this alignment. Residues or secondary structural elements are indicated in a following color code: metal-binding ones, an open black circle; 2OG-binding ones, a filled black circle; DSBH-forming ones, orange. This figure was prepared using ESPript (Robert & Gouet, 2014).

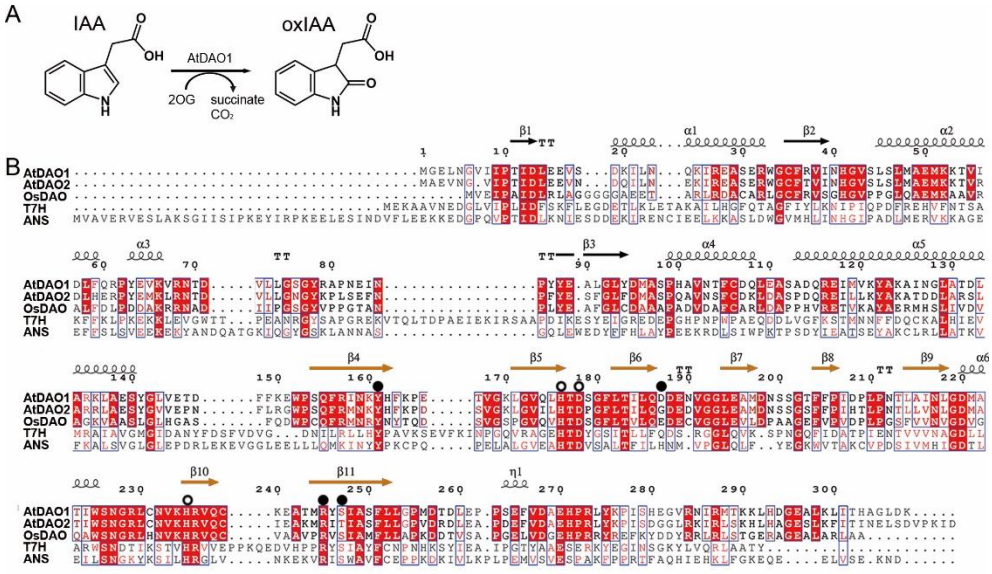
A
IAA
oxIAA
AtDAO1
2OG
succinate
CO2
B
AtDAO1
AtDAO2
OsDAO
T7H
ANS

Materials and Methods

Cloning and purification of AtDAO1 and its mutants

Crystallization of AtDAO1 was successful only after some of N- and C-terminal residues had been removed. Sequence alignment of a full-length, 312 residues AtDAO1 with other members of the 2ODO superfamily suggested that the N- and C-terminal regions are relatively diverse in sequences and, furthermore, the N-terminal region is disordered. Based on these comparisons, I successively truncated residues at both N- and C-termini; Ile9-Pro255, Ile9-Pro277 (Table 1). A full-length AtDAO1, along with truncated ones, were subjected to expression (Fig. 2), purification (Fig. 3), and crystallization (Fig. 4). A crystal of full-length AtDAO1 was not reproduced and AtDAO1 spanning from Il9 to Pro255 was insoluble. Finally, AtDAO1 spanning from Ile9 to Pro277, which is referred AtDAO1* in this study, produced a crystal yielding a high-resolution structure. Later, I validated using in vitro assay that AtDAO1* is catalytically equivalent to the full-length AtDAO1 (see below).

Gene for AtDAO1* was amplified by PCR using a codon-optimized synthetic full-length gene (Bioneer, Korea) as a template. The PCR product was cloned into a pET41 expression vector (Merck) with the C-terminal His-tag, and *Escherichia coli* BL21 (DE3) (Novagen) was then transformed with the resulting plasmid. E coli cells harboring a gene for AtDAO1* were incubated in LB medium at 37°C with 50 μg/ml kanamycin until absorbance at 600 m became about 0.8. Expression of AtDAO1* was induced with 0.5 mM IPTG and cells were further cultured at 20°C for overnight. Cells were collected, sonicated, and centrifuged in

buffer A (50 mM Tris, pH 8.0, 100 mM NaCl, and 2 mM $MgCl_2$). The C-terminal His-tagged AtDAO1* was purified by affinity chromatography using HisTrap HP column (GE Healthcare) with buffer A and eluted using buffer B (buffer A plus 500 mM imidazole). The protein was further purified by size-exclusion chromatography using Superdex-200 (GE Healthcare) with buffer A.

Table 1. Primers for AtDAO1 and its mutants.

Forward	AGTCCATATGGGCGAGCTGAACG
Reverse	AGTCCTCGAGTTTATCCAGGCCGGCGTGA
Primers for truncation	
I9_F	GGAGATATACATATGATCCCGACCATTGACCTTGA
P255_R	GTGGTGGTGCTCGAGCGGGCCCAGCAGGAAAGACG
P277_R	GTGGTGGTGCTCGAGAGGTTTATACAGACGCGGAT
Primers for activity assay	
G75P_F	ACCGATGTGCTGCTG**CCT**TCCGGTTACCGTGCA
G75A_F	ACCGATGTGCTGCTG**GCT**TCCGGTTACCGTGCA
S76A_F	GATGTGCTGCTGGGT**GCC**GGTTACCGTGCACCT
R79K_F	CTGGGTTCCGGTTAC**AAG**GCACCTAACGAAATT
R79A_F	CTGGGTTCCGGTTAC**GCT**GCACCTAACGAAATT
Y88F_F	GAAATTAACCCTTAC**TTT**GAAGCGCTGGGCCTG
Y88A_F	GAAATTAACCCTTAC**GCT**GAAGCGCTGGGCCTG
Q155N_F	AAAGAGTGGCCAAGC**AAT**TTCCGTATTAATAAA
Q155A_F	AAAGAGTGGCCAAGC**GCG**TTCCGTATTAATAAA
R157K_F	TGGCCAAGCCAGTTC**AAG**ATTAATAAATACCAT
R157A_F	TGGCCAAGCCAGTTC**GCT**ATTAATAAATACCAT
Y161A_F	TTCCGTATTAATAAA**GCC**CATTTTAAACCTGAA
H176A_F	CTGGGCGTGCAACTG**GCC**ACGGATTCGGGCTTC
D178A_F	GTGCAACTGCACACG**GCT**TCGGGCTTCCTGACT
S179A_F	CAACTGCACACGGAT**GCG**GGCTTCCTGACTATC
H235A_F	CTGTGCAACGTAAAA**GCC**CGCGTCCAGTGCAAG
R245K_F	AAGGAAGCAACCATG**AAG**TACTCTATCGCGTCT
R245A_F	AAGGAAGCAACCATG**GCT**TACTCTATCGCGTCT
S247A_F	GCAACCATGCGTTAC**GCT**ATCGCGTCTTTCCTG
F251A_F	TACTCTATCGCGTCT**GCC**CTGCTGGGCCCGATG
L253A_F	ATCGCGTCTTTCCTG**GCG**GGCCCGATGGACACC

Sequence are described from 5' to 3'. For mutagenic primers, only forward versions are listed. Underlined sequences indicate restriction sites, and bold-underlined sequences indicate mutated sequences.

Figure 2. The SDS-PAGE analysis of AtDAO1 and its mutants.

Total cell lysates of *Escherichia coli* with or without IPTG induction state on each lane: lane M, protein molecular weight marker, 97, 66, 45, 30, 20, 14 kDa; lane C, control, *E. coli* uninduced; lane T, total, IPTG induction; lane S, soluble fraction. The lysis buffer consists of 50 mM Tris, pH 8.0, 100 mM NaCl, and 2 mM $MgCl_2$. (*A*) Full-length AtDAO1 is soluble. (*B*) AtDOA1* is soluble. (*C*) AtDAO1 spanning from Ile9 to Pro255 is insoluble.

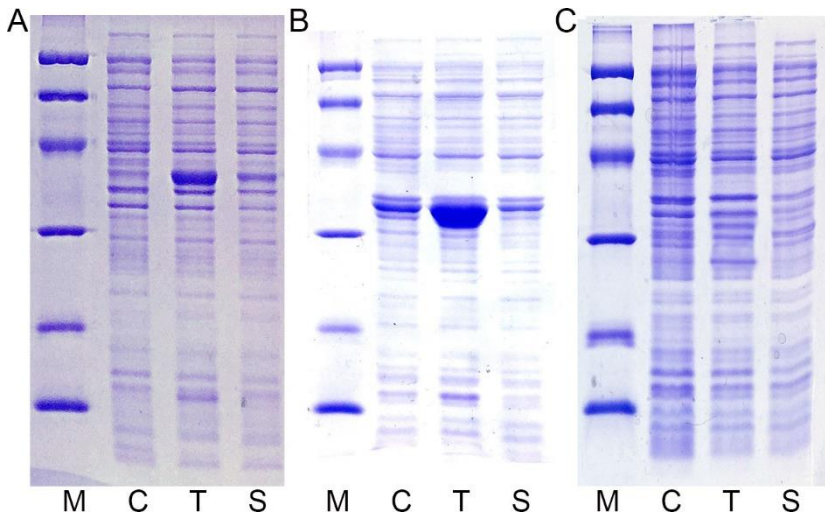
A
B
C
M C T S
M C T S
M C T S

Figure 3. The purification profiles of AtDAO1 and AtDAO1*.

(*A*) With line of absorbance recording at 280nm (blue) and concentration of buffer B (green), AtDAO1 was eluted on HisTrap HP column (GE Healthcare) using the buffer A (50 mM Tris, pH 8.0, 100 mM NaCl, and 2 mM $MgCl_2$) and buffer B (buffer A plus 500 mM imidazole). (*B*) AtDAO1* was also eluted identically to AtDAO1. (*C*) For analysis of AtDAO1* (black; 269 residues) and the full-length AtDAO1 (red; 312 residues), each protein was eluted on Superdex 200 column (GE Healthcare) using the buffer of 50 mM Tris, pH 8.0, 100 mM NaCl, and 2 mM $MgCl_2$. In an insert, molecular weight measurement of elution profiles was compared to 12 ~ 200 kDa molecular mass markers (Sigma Chemical). Note that a void volume corresponds to 45.4 mL, and the eluted peak corresponds to a monomer.

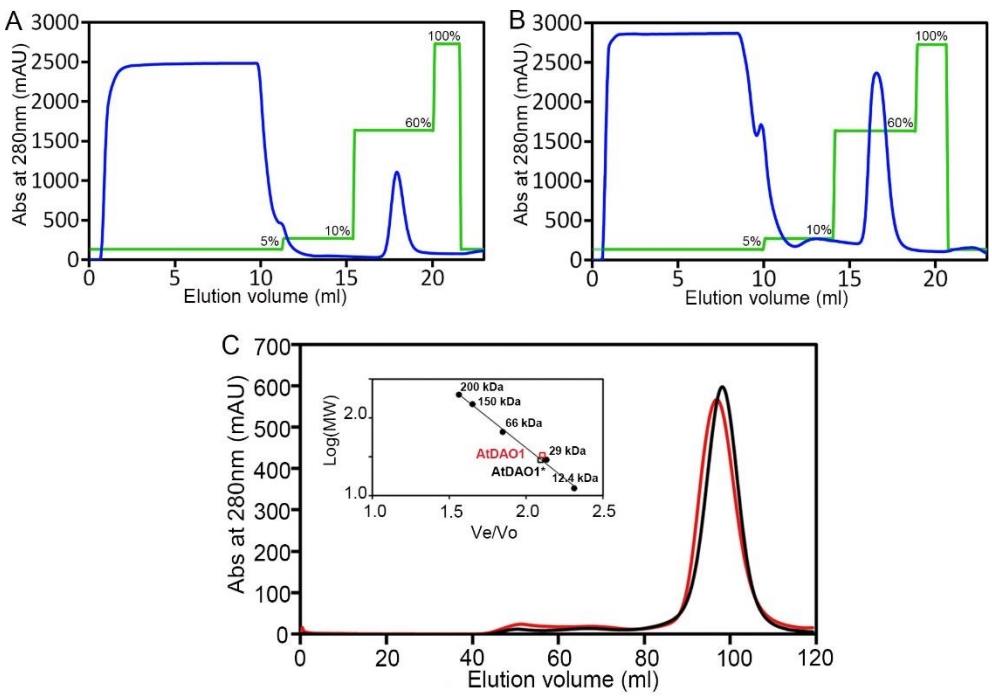
A
B
C
Abs at 280nm (mAU)
Elution volume (ml)
5%
10%
60%
100%
Log(MW)
Ve/Vo
200 kDa
150 kDa
66 kDa
29 kDa
12.4 kDa
AtDAO1
AtDAO1*

Figure 4. The crystal of AtDAO1 and AtDAO1*.

(*A*) Crystals of AtDAO1 were obtained under a crystallization solution of 0.1 M imidazole, pH 8.0, 0.2 M NaCl and 1.0 M $(NH_4)_2HPO_4$. These crystals were not reproduced. (*B*) Crystals of AtDAO1* were obtained under a crystallization solution of 30 mM KH_2PO_4, 16 % PEG8000 and 20 % glycerol.

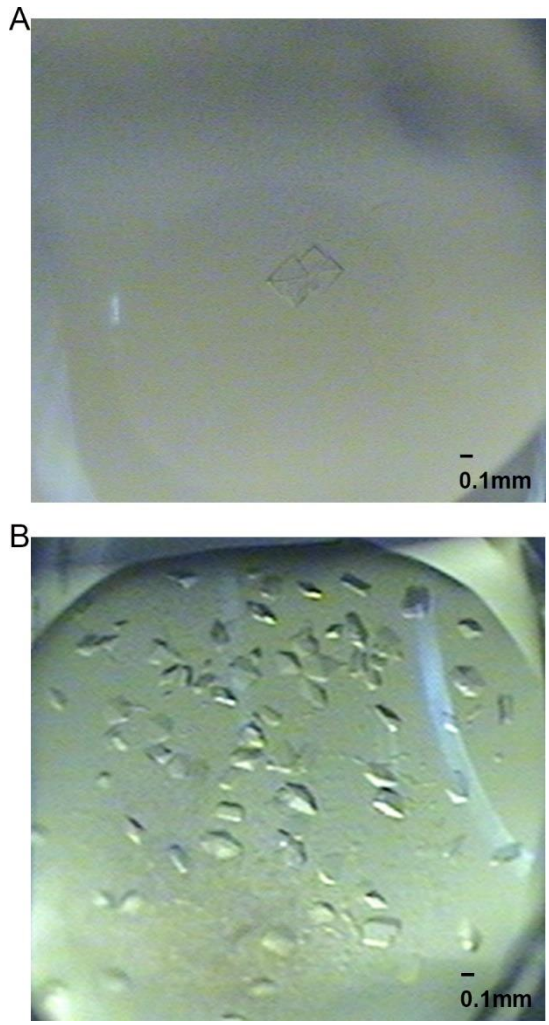
A
0.1mm
B
0.1mm

Crystallization and data collection

Purified AtDAO1* was concentrated to 10 mg/ml and then subject to crystallization using the sitting drop vapor diffusion method at 22°C. Crystals of an unliganded AtDAO1* and a co-crystal of AtDAO1* with 1 mM 2OG were produced in a crystallization solution containing 30 mM KH_2PO_4, 16 % PEG8000 and 20 % glycerol. X-ray diffraction data were collected at 100K on beamline 7A at the Pohang Accelerator Laboratory (Korea) with a 0.5° oscillation angle (Fig. 5). Collected date were processed by HKL2000 (Otwinowski & Minor, 1997), and the high-resolution cutoff was based on a $CC_{1/2}$ statistical value (Winn et al., 2011; Karplus & Diederichs, 2012; Diederichs & Karplus, 2013). Subsequently, I noticed a crystal twining of AtDAO1* using the PHENIX Xtriage utility (Zwart et al., 2005), and determined a twin law for the *pseudo*-merohedrally twinned crystals in the space group $P2_12_12_1$. In particular, the twin operator (*k, h, -l*) was applied for refinement, and the refined twin fraction was found to be 0.05. All crystals belong to the space group $P2_12_12_1$, with three monomers in the asymmetric unit.

Figure 5. The diffraction pattern of AtDAO1*.

Diffraction image of AtDAO1* at 0°. The data are used to determine the crystal's atomic structure. An exposure time was 20 min. During the exposure time, the crystal rotates about 0.5 degrees.

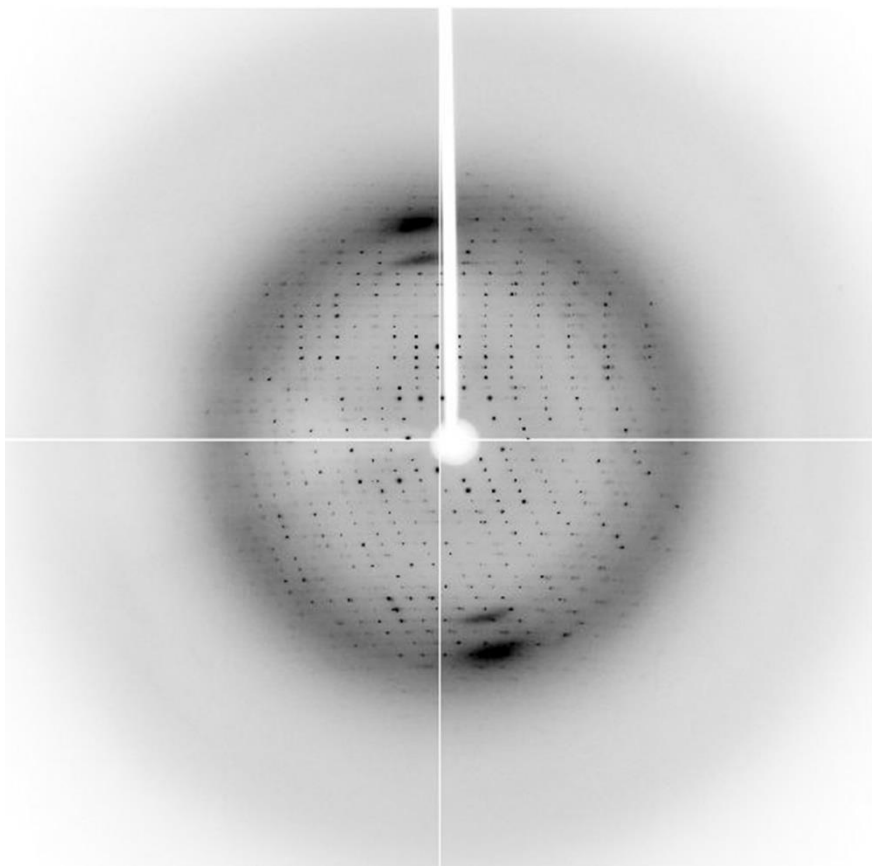

Structure determination and refinement

Structure of an unliganded AtDAO1* was solved by using the PHENIX AutoMR program (Adams et al., 2010). In particular, the Sculptor (Bunkóczi & Reed, 2011) and Ensembler (Terwilliger et al, 2007) utilities in PHENIX were used to generate a search model using a structure of thymine-7-hydroxylase (PDB id 5C3Q; Li et al., 2015) and anthocyanidin synthase (PDB id 2BRT; Welford et al., 2005). Rounds of manual fitting and refinement were conducted with the program COOT (Emsley et al., 2010) and PHENIX twin refinement. Structure of AtDAO1* complexed with 2OG was subsequently refined using a structure of unliganded AtDAO1* as a starting model. The details for data collection and the refinement statistics are in Table 2.

Table 2. Data collection and refinement statistics.

Data set PDB ID	AtDAO1* 6A7R	AtDAO1* complex with 2OG 6A7Q
Data collection		
Wavelength (Å)	0.97933	0.97933
Resolution (Å)	50.0 - 2.08 (2.16-2.08)[a]	50.0 - 2.48 (2.57-2.48)
Unique reflections	56,807 (3,898)	34,716 (3,206)
Multiplicity	7.2 (7.1)	7.1 (7.3)
Completeness (%)	96.4 (67.1)	98.8 (92.4)
Mean I/sigma(I)	11.7 (1.2)	11.6 (0.8)
Wilson B-factors (Å^2)	45.8	64.5
R-merge	0.101 (1.67)	0.126 (3.77)
$CC_{1/2}$[b]	0.998 (0.472)	0.996 (0.500)
Space group	$P2_12_12_1$	$P2_12_12_1$
Unit cell a, b, c (Å)	75.5, 76.6, 165.3	75.9 76.8, 166.3
α, β , γ (º)	90, 90, 90	90, 90, 90
Refinement		
R-work[c]	0.258	0.258
R-free[d]	0.281	0.274
No. of atoms		
Macromolecules	5909	6063
Ligands	3	13
Water	144	49
RMS(bonds) (Å)	0.005	0.005
RMS(angles) (º)	1.12	1.16
Ramachandran favored (%)	97.7	94.4
Ramachandran outliers (%)	0.4	0.5
Average B-factors (Å^2)		
Macromolecules	67.1	84.4
Ligands	71.3	82.5
Water	57.7	66.9

[a]Numbers in parentheses refer to data in the highest resolution shell.

[b]The $CC_{1/2}$ is the Pearson correlation coefficient (CC) calculated from each subset containing a random half of the measurements of unique reflection

[c]$R_{work} = \Sigma \, ||F_{obs}|-|F_{cal}|| / \Sigma |F_{obs}|$

[d]R_{free} is the same as R_{obs} for a selected subset (5%) of the reflections that was not included in prior refinement calculations.

***In vitro* activity assay using LC-MS/MS**

In order to identify residues involved in the substrate specificity of AtDAO1 towards a prime substrate IAA, I carried out LC-MS/MS analyses of oxIAA produced by each variant of AtDAO1. In brief, an enzyme-dependent oxIAA production was performed according to the procedures previously described (Zhang et al., 2016), and quantification of oxIAA was performed relative to an indole-3-propionic acid included in the reaction mixture as an internal standard.

For enzyme assay, various AtDAO1s with the C-terminal His-tag were purified. Gene for each enzyme was amplified by PCR using the full-length AtDAO1 as a template, with respective mutagenic primers (Table 1). Each AtDAO1 variant was then expressed as described above, and purification was carried out by affinity chromatography using HisTrap HP followed by a desalting procedure using HiPrep 26/10 (GE Healthcare) column with buffer of 40 mM PBS (pH 7.4).

Enzyme reaction was carried out according to the procedures described (Zhang et al, 2016). Specifically, a 500 μL reaction mixture includes 40 mM PBS, pH 7.4, 0.5 mM $Fe(SO_4)_2$, 5 mM 2OG, 0.002 mg/ml (*i.e.,* 11.4 μM) IAA in methanol, and 0.35 μM AtDAO1 variant of interest. After 1 hr incubation at 30°C, the reaction was stopped by adding to the mixture 1 ml acetone containing 0.001 mg/mL (*i.e.*, 5.3 μM) indole-3-propionic acid. Subsequently, the resulting reaction mixture was stored at – 20°C for overnight and then subjected to centrifugation at 12,300 × g for 10 min. The supernatant was dried with speed vacuum and resuspended with 50 μL 10 % (v/v) methanol and 0.3 % (v/v) acetic acid.

LC-MS/MS analyses were carried out by pesticide chemistry and toxicology laboratory of Jeong-Han Kim and Yongho Shin.

Results

Overall structure of an unliganded AtDAO1*

Under my crystallization conditions with AtDAO1* lacking eight and thirty-five residues at N- and C-terminal region, respectively, three monomers are arranged in a three-fold symmetric manner in the asymmetric unit (Fig. 6). Size-exclusion chromatographic analysis however indicated that AtDAO1* as well as the full-length (*i.e.*, 312 residues) AtDAO1 remain in solution as a monomeric protein (Fig. 3C), suggesting that trimerization of AtDAO1* is a possible crystallographic artifact. Those three monomers are essentially identical in structure, with a root-mean standard deviation (RMSD) of 0.61–0.98 Å for 259–266 Cα atoms. In this study, I describe the structure of one particular monomeric AtDAO1* with a higher quality of electron density among three monomers.

A 2.09 Å-resolution structure of AtDAO1* includes Ile9 to Leu274, with additional methionine residue at the N-terminus but absence of highly disordered C-terminal three residues and the His-tag. Its overall structure resembles a typical architecture for 2ODOs (Aik et al, 2102; McDonough et al., 2010), in that a double-stranded β-helix (DSBH) or jelly-roll fold is a central structural motif, with α-helical and β-strand extensions around the core DSBH domain (Fig. 7A). AtDAO1* is composed of 6 α-helices and 11 β-strands (Fig. 1B), with eight β-strands (β4–β11) being as DSBH. Specifically, the core DSBH consists of two layers of four-stranded antiparallel β-sheet in a face-to-face orientation, generating cavity in the interior of motif. In AtDAO1*, four antiparallel β-strands form one β-sheet in a β4-11-6-9 order, while antiparallel β-strands in a β5-10-7-8 order represent the other β-sheet. In

structures of 2ODOs, one particular β-sheet in DSBH has further structural extensions by β-strands and is therefore referred to as the major β-sheet, with another DSBH β-sheet being called a minor (Aik et al, 2102; McDonough et al., 2010). In AtDAO1*, three additional β-strands involving β1, β2, and β3 are provided by the N-terminal region (Fig. 1B), and those are associated with both ends of one particular DSBH β-sheet, resulting in the major DSBH β-sheet, with seven β-strands in a β3-4-11-6-9-2-1 order, and all in an antiparallel orientation, except for β1 (Fig. 7A). It is notable that the major DSBH β-sheet in most 2ODOs consists of eight β-strands and the missing eighth β-strand in AtDAO1* corresponds to the loop between α3 and β3.

In addition to these three β-strands, the N-terminal region preceding the DSBH motif also contains five α-helical elements mainly wrapping the major DSBH β-sheet (Fig. 1B and 7A). In particular, those N-terminal α-helices are clustered on the exposed facet of the major β-sheet, the side across from minor one, contributing to stabilization of the overall structure by mediating extensive interactions, mainly hydrophobic interactions, with the major β-sheet. Specifically, two α-helices such as α2 and α5, almost antiparallel to each other, are main elements, while the remaining α1, α3, and α4 locally stabilize β1 and β3, respectively. A 15-residues-long α2 runs almost horizontally from one (*i.e.*, β2) to the other (*i.e.*, β3) end of the major DSBH β-sheet, and a 28-residues-long α5 again transverses in a reverse direction of α2 across the entire facet of a major DSBH β-sheet. In this study, my structural description on the C-terminal region is limited, given that the C-terminal thirty-five residues after Pro277 were removed for crystal formation, but catalytic activity of AtDAO1* is measured to be almost equal to that of the full-length AtDAO1 (see below), suggesting that the C-terminal region is not directly involved in catalysis. It

is also notable that a segment of the C-terminal residues from Pro263 to Arg273 was assigned as a DAO motif unique to the DAO family (Zhang et al., 2016). In AtDAO1*, the motif is associated with a high quality of electron density, and is located on the surface of the minor DSBH β-sheet. Currently, I could not suggest any functional role of the DAO motif.

In summary, an overall architecture of AtDAO1* could be described in a following conceptual way; three layers of structural elements constitute AtDAO1*, in which the major DSBH β-sheet is sandwiched between an N-terminal α-helical layer and a minor DSBH β-sheet. In particular, there are two possible openings of DSBH, each at two ends of DSBH β-sheets near β4 and β9, respectively, but presence of N-terminal extension β1 and β2 seals off effectively a possible opening near β9 in the major β-sheet. Therefore, AtDAO1* exhibits an opening near a major β4 in DSBH that is accessible from solvent and should serve as an entrance to the cavity in DSBH.

Figure 6. The asymmetric unit of AtDAO1*.

Under my crystallization conditions with AtDAO1*, three monomers are arranged in a three-fold symmetric manner in the asymmetric unit. Because of similarity among monomers, different colors were applied to distinguish monomers (magenta, green, cyan).

Figure 7. The overall structure of AtDAO1* and 2OG-binding site.

(*A*) The overall structure of an unliganded AtDAO1* is shown. Different color codes are used for presentation: the major DSBH β-sheet, orange; the minor DSBH β-sheet, green; α-helix, magenta; metal, a black sphere. In this view, an opening to the active site in the DSBH cavity is orientated towards readers. (*B*) Zoomed-in view for the 2OG-binding site is shown in a structure of AtDAO1* in complex with 2OG. An opening to the DSBH cavity is also displayed, with 2OG (green) and metal (black sphere). The 2OG-binding site is located in the DSBH cavity. The metal-binding residues (His176, Asp178, His235) and the 2OG C-5 carboxylate-binding residues (Tyr161, Asp187, Arg245, Ser247) are presented. Note that an orientation is similar with that in Fig. 7A, and therefore the side chains for the metal-binding site project from a ceiling of the cavity. (*C*) Bound 2OG shown in Fig. 7B is overlaid with a 2Fo-Fc electron density map contoured at 1.0 σ.

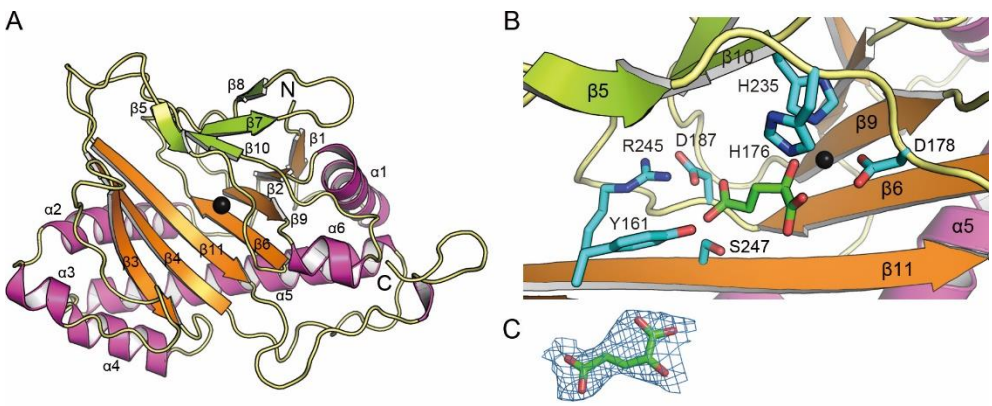
A
β8
N
β5
β7
β1
β10
α1
β2
α2
β9
α6
β11
β6
β4
β3
α3
α5
C
α4
B
β10
β5
H235
β9
R245
D187
H176
D178
β6
Y161
α5
S247
β11
C

Active site of AtDOA1*

In AtDAO1*, I identified a binding site of metal ion in the active site (Fig. 8), based on its coordinating distance and geometry, as well as its positional resemblance with those of other 2ODOs (Aik et al, 2102; McDonough et al., 2010). Currently, magnesium ion is assigned as a possible cation at the iron-binding site, given that under my aerobic experimental conditions Mg(II) ion is included in buffer for protein purification or crystal formation to avoid an encountered oxidation problem of Fe(II) ion. It is located just on the border region for an entrance to the DSBH cavity (Fig. 7A). In particular, a major β4 and a minor β5 in DSBH are an entrance to the active site, and an extension β3 and its preceding loop apparently serve as a part of platform for a prime substrate binding. Magnesium ion is coordinated within 2.4 Å with residues highly conserved in the 2ODO family (Fig. 1B): His176, Asp178, and His235. These metal-binding residues, called as the Hx(D/E)…H motif, represent a hallmark for the 2ODO family, and are located at a loop between a minor β5 and a major β6, and at an edge of a minor β10, a ceiling of the cavity, with their side chains projecting inward to cavity.

I further carried out co-crystal formation of AtDAO1* with the co-substrate 2OG under aerobic environment. Crystallization conditions and all other crystallographic features are identical with those of the unliganded AtDAO1*. Among three monomers, only one exhibits a binding of 2OG (Fig. 7B and C). The binding mode of 2OG is similar with those in other 2ODOs utilizing 2OG as co-substrate (Aik et al, 2102; McDonough et al., 2010). The 2OG C-1 carboxylate anchors at the metal-binding site and the C-5 carboxylate is swung in and bound to further inside of the cavity. Specifically, the 2OG C-1 carboxylate and 2-oxo mediate bidentate coordination within 2.4 Å with the bound metal, while its C-5 carboxylate

group points towards the interior of DSBH cavity and forms several electrostatic or hydrogen bonds in a distance of 3.4 Å with Tyr161, Asp187, Arg245, and Ser247, residues conserved among the 2ODO family (Fig. 1B and 7B). Therefore, binding of a metal ion and a co-substrate 2OG is mediated by the highly conserved residues among the 2ODO family that are located at an entrance or in a deeper inside of DSBH cavity. Under these structural circumstances, the binding of a prime substrate IAA should occur at the region anterior to the metal-binding site.

Figure 8. The structure of metal-binding site in the active site of the unliganded. This orientation is almost identical with that in Fig. 7B. The metal ion in a black sphere, and the metal-binding residues His176, Asp178, and His235 are presented, with a 2Fo-Fc electron density map contoured at 1.0 σ.

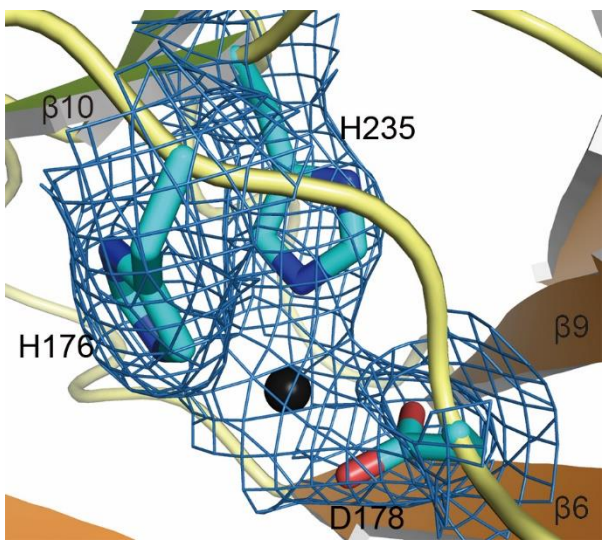
β10
H235
H176
β9
D178
β6

Putative binding site for IAA in AtDOA1

It is not unexpected that given high sequence homologies of the essential residues, general structural features for the active site and the binding environments of a co-substrate 2OG in AtDAO1* are well conserved among members of the 2ODO family. Rather, critical issues for AtDAO1 are structural determinants for the substrate specificity towards a prime substrate IAA. Further trial to form a ternary complex of AtDAO1* with 2OG and substrate IAA, or soaking experiments with IAA has been unsuccessful. Therefore, I analyzed a putative site for IAA-binding in AtDAO1* by comparing AtDAO1* structure with other 2ODOs in complex with 2OG and its prime substrate.

Structural homology search program DALI (Holm & Rosenstrom, 2010) suggested that AtDAO1* is most similar with thymine-7-hydroxylase (PDB id 5C3Q; Li et al., 2015) and anthocyanidin synthase (PDB id 2BRT; Welford et al., 2005), with Z-score of more than 28. Those three structures, all in the 2ODO family, are aligned, with a RMSD of 1.8–1.9 Å for 242–243 Cα atoms. Further comparisons indicate that the binding mode of 2OG is conserved in these structures, but there are notable variations in structure and sequence for the binding site of a prime substrate (Fig. 1B and 9). In general, a prime substrate, thymine in thymine-7-hydroxylase and naringenin in anthocyanidin synthase, is bound to a groove that is in position anterior to an entrance to the DSBH cavity, and is surrounded by several structural elements including major β3, β4, β11, and their associated loop regions. Specifically, many residues emanated from β3 and β4 on the edge of a major DSBH β-sheet remain relatively well exposed and thus provide a platform for various interactions. In addition to this platform, three different loops and their associated regions apparently project towards the anterior area, thereby resulting in a groove for the substrate-

binding site (Fig. 9). Those loops contain the N- or C-terminal regions, and are ones following α3 (*i.e*., Loop-I), preceding β3 (Loop-II), and following β11 (Loop-III), respectively. It is noteworthy that the length and/or sequence of those loops are specific to each member of the 2ODO family (Fig. 1B), suggesting that dimension and geometry of the groove is unique to each member and thus plays a role in dictating a specificity towards the prime substrate.

My structural comparisons exhibit following major features for the prime substrate-binding site; (i) the platform-forming residues, mainly in a major β3, β4, and β11, are relatively conserved for their hydrophobic or hydrophilic features in the 2ODO superfamily, (ii) the length and sequence of three loops in the site is diverse among members of the 2ODO family but well conserved in the DAO-family, and (iii) loop conformations are different, but apparently influenced by the size or shape of a prime substrate. Therefore, in the prime substrate-binding site, loops showing variations in sequence or in conformation, compared with other 2ODOs, could account for characteristic of AtDAO1. I recognized in AtDAO1* that loop-I and –II show diversities in conformation and sequence, respectively (Fig. 9). Specifically, AtDAO1* loop-I adopts a conformation similar to that of thymine-7-hydroxylase in the presence of small-size prime substrate (*i.e.,* thymine), but is completely different from that with a relatively larger one (*i.e.,* naringenin) in anthocyanidin synthase (Fig. 8). Loop-II in AtDAO1* is relatively short about 8 residues, compared with 27- and 13-residues-long loop in thymine-7-hydroxylase and anthocyanidin synthase, respectively. This region has been recognized to be characteristic of each member of the 2ODO family (Aik et al., 2012). Unlike loop-I and –II, conformation of loop-III is relatively conserved.

Figure 9. The superimposed structure of AtDAO1* with the 2ODO family.

The prime substrate-binding site is presented with a stereo view. In this presentation, three structures are superimposed including AtDAO1* (red), thymine-7-hydroxylase (blue; PDB id 5C3Q) and anthocyanidin synthase (green; PDB id 2BRT), with the metal-site (black sphere) of AtDAO1* and a respective prime substrate, thymine (purple) for thymine-7-hydroxylase and naringenin (yellow) for anthocyanidin synthase. The side chains of AtDAO1* are indicated for their possible involvements in an IAA-binding and further subject to mutagenesis for functional analyses. These structures are well aligned in the DSBH motif, including a metal site, but show noticeable variations in conformations of the loops regions proximal to a prime substrate-binding site.

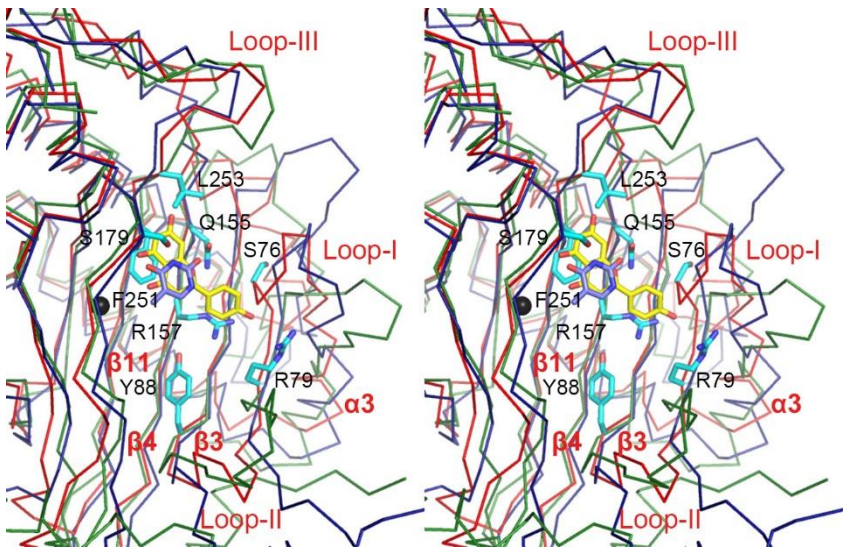
Loop-III
L253
Q155
S179
S76
Loop-I
F251
R157
β11
Y88
R79
α3
β4
β3
Loop-II
Loop-III
L253
Q155
S179
S76
Loop-I
F251
R157
β11
Y88
R79
α3
β4
β3
Loop-II

In vitro activity assay of AtDAO1 and its mutants

I selected a total of fifteen residues for site-directed mutagenesis, and twenty-one mutants were designed to validate or characterize their functional roles: His176, Asp178, His235 for the metal-coordinating residues (Fig. 7B); Tyr161, Asp187, Arg245, Ser247 for 2OG C-5 carboxylate-interacting residues (Fig. 7B); Gly75, Ser76, Arg79 for Loop-I region; Tyr88 for Loop-II region; Gln155, Arg157 from β4; Ser179 from β5; Phe251, Leu253 from β11 (Fig. 9). Specifically, the loop-I and -II residues with their side chains projecting towards a groove are selected, mainly due to their possible proximity to a prime substrate IAA. Except for Ser179 from β5, other residues from major β-strands are at the bottom of platform, on which a prime substrate could sit on (Fig. 9). The residues mediating interactions with a metal ion and 2OG C-5 carboxylate group are strictly conserved among the 2ODO family, but many residues for a prime substrate-binding site are specific for AtDAO1 or DAO subfamily (Fig. 1B).

In vitro activity of each mutant was assayed by measuring production of oxIAA using LC-MS/MS analysis, and the resulting activity was compared with the wild-type AtDAO1 (Fig. 9). First, I noticed that AtDAO1* used for structure determination in this study exhibits activity almost equal to the full-length enzyme, suggesting that the C-terminal region beyond Pro277 is not critical for AtDAO1 activity. Mutation of the Fe(II)-coordinating and 2OG C-5 carboxylate-interacting residues impaired their catalytic activities, consistent with their functional roles. Specifically, except for H235A mutant showing 43% activity of the wild-type AtDAO1, mutants for the metal-coordinating residues, H176A and D178A, show 10% and 28% activity, respectively, while 10–20% activity was measured for Y161A, R245K, and R245A mutant, with about 67% activity for S247A.

Mutation for a prime substrate-binding site exhibits some interesting features. In general, mutants for the platform region are generally tolerant to mutation and do not cause significant influences on activity, relative to those for the loop regions. About 41–114% of activity was observed for mutants of the platform residues, but those activities for mutants of the loop residues are reduced to 24–66% of the wild-type AtDAO1. It is notable that mutation of the DAO-specific residues (Fig. 1B), including Gly75, Tyr88, Ser179, causes detrimental effects on activity, except for Phe251 also conserved in other 2ODO members. Specifically, in the loop-I region, the chemical identity of Gly75 and Arg79 appears to be important for enzyme function. Unlike a similar activity for G75P (27%; percentage in parenthesis corresponds to a relative activity of AtDAO1) and G75A (24%) mutant, R79A (31%) lost its efficacy considerably relative to R79K (66%) (Fig. 10A), suggesting the functional role of the positively charged residue at that location. A possible hydrogen bond at Tyr88 in the loop-II region likely plays an important role in enzyme function, with Y88F(37%) and Y88A(41%), indicating that mutational effects caused by removing the side chain hydroxyl group from tyrosine are almost equal to those of alanine replacement.

Mutants in the platform region also deliver some clues to their functional roles. Residues such as Gln155, Arg157, and Phe251 form a bottom layer for interactions with a prime substrate (Fig. 8). However, I could not propose any functional role of Gln155 and Phe251, with Q155N (55%), Q155A (102%), and F251A (115%) mutant. The positive charge on Arg157 rather plays an important role, based on observation that R157K (101%) restores its activity relative to R157A (50%). The chemical identity of these three residues are highly conserved in the 2ODO family, as well as in the DAO family (Fig. 1B), suggesting their general roles

in a dioxygenase reaction. Ser179 and Leu253 are unique to the DAO family, and chemical nature of the structurally equivalent residues in other enzymes is quite different as indicated in sequence alignment (Fig. 1B): tyrosine and asparagine in thymine-7-hydroxylase, and valine and glutamate in anthocyanidin synthase, respectively. Mutation caused moderate effects on the enzyme activity, with S179A (47%) and L253A (41%).

In a previous study of thymine-7-hydroxylase, mutagenesis and a binding assay using an isothermal calorimeter indicated that Phe292, Tyr217, and Arg190 corresponding in structure to Phe251, Ser179, and Arg157 in AtDAO1 are important in substrate biding and catalysis (Li et al., 2015). Mutation of those three residues in thymine-7-hydroxylase impaired significantly enzyme activity, but those mutational effects were not observed in my mutational analyses of the corresponding residue (Fig. 10A), suggesting that the binding mode of a prime substrate in thymine-7-hydroxylase could differ from that of IAA in AtDAO1. In the absence of structural information for AtDAO1* complexed with IAA, I could not assign a specific functional role of each residue tested for in vitro activity assay. However, mapping mutational effects on residues displays that residues in the loop-I and loop-II region play an important role in enzyme function (Fig.10B and C), leading me to propose that structural determinants in AtDAO1 for the IAA specificity are originated from sequences and conformation of the loop and their nearby regions in the prime substrate-binding site. In particular, those loop residues are thought to be proximal to IAA, and relatively well conserved among the DAO family but not in the 2ODO family, consistent with their possible roles for IAA recognition.

Figure 10. The putative binding site of IAA and LC-MS/MS analysis of oxIAA. (*A*) *In vitro* activity of AtDAO1 and its mutants. In the assay, production of oxIAA was measured using LC-MS/MS and quantified relative to an indole-3-propionic acid included in the assay as an internal standard. Those values are compared to that of the wild-type AtDAO1. Different color codes are indicated: green, the wild-type AtDAO1 and AtDAO1*; red, the metal-binding residues; blue, the 2OG C-5 carboxylate-binding residues; yellow, the putative prime substrate-binding residues. Each measurement was carried out in triplicate, with an error bar. (*B*) Surface representation is shown for the overall structure of AtDAO1*. This structure is almost identical with Fig. 10C. (*C*) Surface representation is shown for the prime substrate IAA-binding site in AtDAO1*. This orientation is almost identical with Fig. 9. The surface of residues is indicated in a different color, depending on its resulting activity by mutation: magenta, residues with less than 40% activity; cyan, 40–60% activity; white, more than 60% activity. Note that residue with two independent mutants (see Fig. 10A) is based on a mutant with a lower activity.

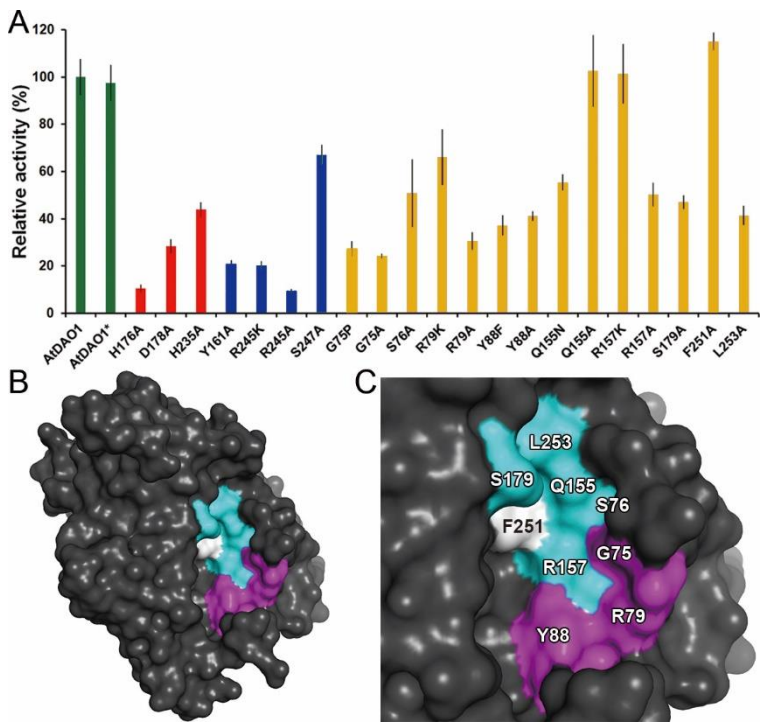
A
Relative activity (%)
120
100
80
60
40
20
0
AtDAO1
AtDAO1*
H176A
D178A
H235A
Y161A
R245K
R245A
S247A
G75P
G75A
S76A
R79K
R79A
Y88F
Y88A
Q155N
Q155A
R157K
R157A
S179A
F251A
L253A
B
C
L253
S179
Q155
S76
F251
G75
R157
R79
Y88

Discussion

In this study, I determined a crystal structure of AtDAO1 and its complex with co-substrate 2OG. The metal- and 2OG-binding site in AtDAO1, as well as its overall structure, is highly homologous with those of the 2ODO family, consistent with high sequence identity of those binding residues. However, variations in both sequence and structure are localized in the loop regions proximal to the prime substrate-binding site. LC-MS/MS analyses of various mutants suggest that structural determinants for the IAA specificity in AtDAO1 emerge from sequences of the loop regions in the prime substrate-binding site. These results provide structural basis of how a plant hormone IAA could be oxidized by AtDAO1, a key enzyme in auxin catabolism.

References

Abel S and Theologis A (2010) Odyssey of auxin. *Cold Spring Harb Perspect Biol* doi: 10.1101/cshperspect.a004572

Adams PD, Afonine PV, Bunkóczi G, Chen VB, Davis IW, Echols N et al. (2010) PHENIX: a comprehensive Python-based system for macromolecular structure solution. *Acta Crystallogr D Biol Crystallogr* 66, 213-221.

Aik W, Mcdonough MA, Tahnlhammer A, Chowdhury R and Schofield CJ (2012) Role of the jelly-roll fold in substrate binding by 2-oxoglutarate oxygenases. *Curr Opin Struct Biol* 22, 691-700.

Bunkóczi G and Read RJ (2011) Improvement of molecular-replacement models with Sculptor. *Acta Crystallogr D Biol Crystallogr* 67, 303-312.

Diederichs K and Karplus PA (2013) Better models by discarding data? *Acta Crystallogr D Biol Crystallogr* 69, 1215-1222.

Emsley P, Lohkamp B, Scott WG and Cowtan K (2010) Features and development of Coot. *Acta Crystallogr D Biol Crystallogr* 66, 486-501.

Hagel JM and Facchini PJ (2018) Expanding the roles for 2-oxoglutarate-dependent oxygenases in plant metabolism. *Nat Prod Rep* doi: 10.1039/c7np00060j

Herr CQ and Hausinger RP (2018) Amazing Diversity in Biochemical Roles of Fe(II)/2-Oxoglutarate Oxygenases. *Trends Biochem Sci* doi: 10.1016/j.tibs.2018.04.002

Holm L and Rosenstrom P (2010) Dali server: conservation mapping in 3D. *Nucleic Acids Res* 38, W545-549.

Karplus PA and Diederichs K (2012) Linking crystallographic model and data quality. *Science* 336, 1030-1033.

Kowalczyk M and Sandberg G (2001) Quantitative analysis of indole-3-acetic acid metabolites in Arabidopsis. *Plant Physiol* 127, 1845-1853.

Li W, Zhang T and Ding J (2015) Molecular basis for the substrate specificity and catalytic mechanism of thymine-7-hydroxylase in fungi. *Nucleic Acids Res* 43, 10026-10038.

Ljung K (2013) Auxin metabolism and homeostasis during plant development. *Development* 140, 943-950.

Mellor N, Band LR, Pencík A, Novák O, Rashed A, Holmana T et al. (2016) Dynamic regulation of auxin oxidase and conjugating enzymes AtDAO1 and GH3 modulates auxin homeostasis. *Proc Natl Acad Sci U S A* 113, 11022-11027.

Mcdonough MA, Loenarz C, Chowdhury R, Cligton IJ and Schofield CJ (2010) Structural studies on human 2-oxoglutarate dependent oxygenases. *Curr Opin Struct Biol* 20, 659-672.

Otwinowski Z and Minor W (1997) Processing of X-ray diffraction data. *Methods Enzymol* 276, 307-326.

Porco S, Pěnčík A, Rashed A, Voß U, Casanova-Sáez R, Bishopp A et al. (2016) Dioxygenase-encoding AtDAO1 gene controls IAA oxidation and homeostasis in Arabidopsis. *Proc Natl Acad Sci U. S. A.* 113, 11016-11021.

Robert X and Gouet P (2014) Deciphering key features in protein structures with the new ENDscript server. *Nucleic Acids Res* 42, W320-324.

Terwilliger TC, Grosse-Kunstleve RW, Afonine PV, Adams PD, Moriarty NW, Zwart PH et al. (2007) Interpretation of ensembles created by multiple iterative rebuilding of macromolecular models. *Acta Crystallogr D Biol Crystallogr* 63, 597-610.

Welford RWD, Clifton IJ, Turnbull JJ, Wilson SC and Schofield CJ (2005) Structural and mechanistic studies on anthocyanidin synthase catalysed oxidation of flavanone substrates: the effect of C-2 stereochemistry on product selectivity and mechanism. *Org Biomol Chem* 3, 3117-3126.

Winn MD, Ballard CC, Cowtan KD, Dodson EJ, Emsley P, Evans PR et al. (2011) Overview of the CCP4 suite and current development. *Acta Crystallogr D Biol Crystallogr* 67, 235-242.

Zwart PH, Grosse-Kunstleve RW and Adams PD (2005) Xtriage and Fest: automatic assessment of X-ray data and substructure structure factor estimation. *CCP4 Newsletter* 42, 10.

Zhang J, Lin JE, Harris C, Pereira FCM, Wu F, Blakeslee JJ et al. (2016) DAO1 catalyzes temporal and tissue-specific oxidative inactivation of auxin in Arabidopsis thaliana. *Proc Natl Acad Sci U S A* 113, 11010-11015.

Zhang J and Peer WA (2017) Auxin homeostasis: the DAO of catabolism. *J Exp Bot* 68, 3145-3154.

Zhao Z, Zhang Y, Liu X, Zhang X, Liu S, Yu X et al. (2013) A role for a dioxygenase in auxin metabolism and reproductive development in rice. *Dev Cell* 27, 113-122.

Abstract in Korean

서울대학교 대학원

농생명공학부 응용생명화학전공

진소희

Indole-3-acetic acid (IAA) 는 식물 호르몬 옥신 (auxin) 의 주요 형태로 식물의 성장과 발달의 거의 모든 부분을 조절한다. 따라서 옥신의 항상성은 식물에서 필수적 주제이다. 옥신의 항상성에는 합성, 수송, 접합 및 이화작용의 다양한 경로가 관여하지만, 최근의 연구에서 벼 *Oryza sativa* 와 애기장대 *Arabidopsis thaliana* 로부터의 *AUXIN OXIDATION FOR DIOXYGEANSE (DAO)* 의 존재가 밝혀질 때까지는 그 대사 경로를 파악하기 어려웠다. 2-oxoglutarate/Fe(II)-dependent oxygenase family 에 속하는 DAO 는 IAA 이화 과정에 주요한 효소이다. AtDAO1 은 2-oxoglutarate 를 보조 기질로 이용하여, IAA 를 기능적으로 비활성이고 산화된 생성물인 2-oxoindole-3-acetic acid 로 전환시킨다. 본 학위논문에서, 기질이 붙지 않은 *A. thaliana* 에서 유래한 DAO1 (AtDAO1) 과 2-oxoglutarate 와 복합체의 결정 구조를 밝히고자 한다. AtDAO1 은 2-oxoglutarate/Fe(II)-dependent oxygenase family 와 구조적으로 유사하지만, 주요 기질 결합 부위에는 독특한 특징을 가진다. 다양한 돌연변이 효소의 반응 생성물인 2-oxoindole-3-acetic acid 를 이용하여 액체 크로마토그래피-이중 질량 분석기로 분석을 함으로써, 가능한 구조적 측면에서 AtDAO1 의 IAA 에 대한 기질 특이성에 대해 제안하고,

주요 기질 IAA 의 추정되는 결합 부위에 대한 구조적 통찰력을 제공한다.

주요어: 애기장대, AtDAO1, dioxygenase for auxin oxidation, indole-3-acetic acid, 2-oxoglutarate, 2-oxoglutarate/Fe(II)-dependent oxygenase family, 2-oxoindole-3-acetic acid

학 번: 2016-24638